JOURNAL OF GEOPHYSICAL RESEARCH, VOL. 105, NO. C2, PAGES 3325–3338, FEBRUARY 15, 2000

Modeling Arctic sea ice with an efficient plastic solution

Jinlun Zhang and Drew Rothrock

Polar Science Center, Applied Physics Laboratory, College of Ocean and Fishery Sciences
University of Washington, Seattle

Abstract. A computationally efficient numerical method is developed for solving sea ice momentum equations that employ a nonlinear viscous-plastic rheology. The method is based on an alternating direction implicit (ADI) technique that involves a direct solution of the momentum equations. This method is therefore more computationally efficient than those employing an iterative procedure in solving the equations. The ADI method for modeling sea ice dynamics is dynamically consistent since it rapidly approaches a viscous-plastic solution described by the sea ice rheology. With different model configurations of varying spatial resolutions and decreasing time step intervals the ADI method converges to the same viscous-plastic solution as another numerical method that uses a line successive relaxation procedure to solve the ice momentum equations. This indicates that the ADI method is also numerically consistent. The approximateness of numerical solutions of sea ice, resulting from coarse model resolutions in time, is addressed. It is found that a significant bias, up to 10% or more, in the solution is likely to occur for a typical but coarse time step interval. This indicates that an assessment of the numerically created bias from a crude time integration may be necessary when model data comparisons are performed. In addition, suggestions are given for selecting appropriate time step intervals to enhance numerical accuracy in model applications.

1. Introduction

In many large-scale sea ice dynamics models the ice motion is described by momentum equations that treat the ice cover as a two-dimensional continuum obeying a certain constitutive law, or rheology. The ice rheology describes the internal interaction of the ice and significantly affects predictions of ice circulation and ice thickness [*Ip et al*., 1991; *Ip*, 1993; *Hibler and Ip*, 1995]. Two predominant ice rheologies have been used in sea ice models to represent ice interaction, which has been long thought to be a complicated, highly nonlinear, physical process. One is elastic-plastic rheology [*Coon*, 1974; *Pritchard*, 1975] and the other viscous-plastic rheology [*Hibler*, 1979]. Although the elastic-plastic models have proven very useful in describing sea ice motion in many applications, they generally require a knowledge of the strain history of the ice cover and small time steps to resolve elastic waves numerically. The viscous plastic model proposed by *Hibler* [1979] has found wide utility in large-scale sea ice modeling because of its relative simplicity and ease of numerical implementation.

The *Hibler* [1979] model uses a semi-implicit numerical method to solve momentum equations that include a nonlinear viscous-plastic rheology with an elliptical yield curve. This method is a combination of a modified Euler time stepping scheme and a point successive relaxation (PSR) procedure. The modified Euler time stepping is rather effective in dealing with the nonlinearity of the plastic rheology and with the water drag obeying a quadratic law and leads to a numerically stable solution. However, the iterative point successive relaxation procedure is rather computationally intensive because of a slow convergence rate and is therefore not efficient for large grids with high resolution.

Paper number 1999JC900320.
0148-0227/00/1999JC900320$09.00

Consequently, a numerical method with a different semi-implicit approach was proposed by *Zhang and Hibler* [1997] (hereinafter referred to as ZH) for solving ice momentum equations. The method is based on decoupling the u and v momentum equations into a form having substantially improved convergence properties and uses a tridiagonal solver in conjunction with a line successive relaxation (LSR) procedure. The ZH method converges especially rapidly and is 12 times more efficient than the PSR method on a particular machine. The ZH method can also simulate an ice cover in a fully plastic flow by taking a number of "pseudo time steps" without drastically increasing computer time. By pseudo time steps we mean that at each physical time step the momentum equations are solved repeatedly with updated calculations of ice rheology (see ZH for details). This is important for either large-scale or small-scale modeling where the interest is in accurate representation of sea ice as a plastic material. Because of its efficiency in computation and accuracy in achieving plastic flow the method has been used in climate studies that are mainly interested in the ice cover's seasonal and interannual variations in response to wind and thermal forcing often in a timescale of days [*Zhang*, 1993; *Zhang et al*., 1998a, b, 1999]. With a number of pseudo time steps this method has also been used in studies that are interested in representing sea ice as a plastic material with rapid transient response to wind forcing [*Ip*, 1993; *Hibler and Ip*, 1995; *Song*, 1994; *Geiger et al*., 1998].

Although the ZH method marks considerable progress in achieving computational efficiency in modeling sea ice dynamics, it involves an iterative LSR procedure. The iterative procedure is still computationally intensive and therefore may not be most desirable for long-term climate simulation and prediction. In this paper, we present a new numerical method for sea ice dynamics that eliminates the iterative LSR procedure adopted in the ZH method. Without iterations the new method conducts a direct solution of the ice momentum equa-

tions. Therefore it achieves higher computational efficiency and is more suitable for climate studies. In addition, this new method, like the LSR method, approaches a fully plastic solution with decreasing time step intervals with or without pseudo time steps, which is important for an accurate prediction of ice motion, deformation, and stress that are described by the viscous-plastic rheology. The new method is presented in section 2, and its behavior is examined in section 3 in comparison with the LSR method. An analysis of the new method's numerical stability is presented in the appendix.

2. Model Description

2.1. Ice Momentum Balance

Sea ice motion is described by the following momentum balance [*Hibler*, 1979]:

$$m(\partial \mathbf{u}/\partial t) = -mf\mathbf{k} \times \mathbf{u} + \tau_a + \tau_w - mg\nabla_H p(0) + \nabla \cdot \sigma, \tag{1}$$

where m is ice mass per unit area, $\mathbf{u}$ is ice velocity, f is the Coriolis parameter, $\mathbf{k}$ is the unit vector in the z direction, τ_a is air drag, τ_w is water drag, g is the acceleration due to gravity, $p(0)$ is sea surface dynamic height, and σ is an ice internal stress tensor (σ_{ij}). The air drag and water drag are given by [see *McPhee*, 1986]

$$\tau_a = \rho_a C_a |\mathbf{U}_g|(\mathbf{U}_g \cos \phi + \mathbf{k} \times \mathbf{U}_g \sin \phi) \tag{2}$$

$$\tau_w = \rho_w C_w |\mathbf{U}_w - \mathbf{u}|[(\mathbf{U}_w - u) \cos \theta + \mathbf{k} \times (\mathbf{U}_w - \mathbf{u}) \sin \theta], \tag{3}$$

where $\mathbf{U}_g$ and $\mathbf{U}_w$ are geostrophic wind and geostrophic ocean current, C_a and C_w are air and water drag coefficients, ρ_a and ρ_w are air and water densities, and ϕ and θ are air and water turning angles. These model constants and parameters are given by *Hibler* [1979]. The last term in (1) represents an internal ice interaction force, with the stress tensor being related to ice strain and strength following the viscous plastic constitutive law.

$$\sigma_{ij} = 2\eta\dot{\varepsilon}_{ij} + (\zeta - \eta)\dot{\varepsilon}_{kk}\delta_{ij} - (P/2)\delta_{ij}, \tag{4}$$

where $\dot{\varepsilon}_{ij}$ is ice strain rate, P is ice strength, and ζ and η are the bulk and shear viscosities. The nonlinear viscosities are based on an elliptical yield curve and are given by

$$\zeta = P/2\Delta \qquad \eta = \zeta/e^2, \tag{5}$$

where $e = 2$ and $\Delta = [(\dot{\varepsilon}_{11}^2 + \dot{\varepsilon}_{22}^2)(1 + e^{-2}) + 4e^{-2}\dot{\varepsilon}_{12}^2 + 2\dot{\varepsilon}_{11}\dot{\varepsilon}_{22}(1 - e^{-2})]^{1/2}$. Clearly, these viscosities are functions of ice strain rate and ice strength and, in order to approximate rigid plastic behavior, are allowed to take on a large maximum value specified by *Hibler* [1979] when the deformation rate becomes very small ($\Delta \to 0$). In such a situation, the sea ice behaves like a linear viscous fluid, with a very slow "creeping," instead of a plastic material.

From the above equations the component equations of (1) in a rectangular coordinate system can be written as

$$m\frac{\partial u}{\partial t} = -Cu + Dv + \frac{\partial}{\partial x}(\zeta + \eta)\frac{\partial u}{\partial x} + \frac{\partial}{\partial y}\eta\frac{\partial u}{\partial y} + \frac{\partial}{\partial x}(\zeta - \eta)\frac{\partial v}{\partial y} + \frac{\partial}{\partial y}\eta\frac{\partial v}{\partial x} + \tau_x \tag{6}$$

$$m\frac{\partial v}{\partial t} = -Cv - Du + \frac{\partial}{\partial y}(\zeta + \eta)\frac{\partial v}{\partial y} + \frac{\partial}{\partial x}\eta\frac{\partial v}{\partial x} + \frac{\partial}{\partial y}(\zeta - \eta)\frac{\partial u}{\partial x} + \frac{\partial}{\partial x}\eta\frac{\partial u}{\partial y} + \tau_y, \tag{7}$$

where $C = \rho_w C_w|\mathbf{U}_w - \mathbf{u}| \cos \theta$, $D = \rho_w C_w|\mathbf{U}_w - \mathbf{u}| \sin \theta + mf$, $\tau_x = \tau_{ax} + \tau_{wx} - (\partial P/\partial x)/2$, and $\tau_y = \tau_{ay} + \tau_{wy} - (\partial P/\partial y)/2$. Note that, like the LSR method, the present new method is also applicable to the momentum equations in any orthogonal curvilinear coordinate system, including those in the spherical coordinate system given by ZH.

2.2. Previous LSR Method

Before we present the new numerical method for solving (6) and (7) we briefly describe the LSR method. The LSR method adopts a three-level time stepping procedure for discretizing (6) and (7); this scheme consists of a two-level modified Euler time step and a third level of correction at each time step. The two-level modified Euler time step is described by (8)–(11), with some derivative terms in (6) and (7) being omitted. The omitted terms are treated the same way in time as the next-to-last term in each equation.

The first level of the modified Euler time step at time step $k + 1$ is written as

$$m\frac{u^{k+1/2} - u^k}{\Delta t} = -C(\mathbf{u}^k)u^{k+1/2} + D(\mathbf{u}^k)v^k + \frac{\partial}{\partial x}E(\mathbf{u}^k)\frac{\partial u^{k+1/2}}{\partial x} + \frac{\partial}{\partial y}\eta(\mathbf{u}^k)\frac{\partial u^{k+1/2}}{\partial y} + \frac{\partial}{\partial x}\zeta(\mathbf{u}^k)\frac{\partial v^k}{\partial y} + \tau_x(\mathbf{u}^k) \tag{8}$$

$$m\frac{v^{k+1/2} - v^k}{\Delta t} = -C(\mathbf{u}^k)v^{k+1/2} - D(\mathbf{u}^k)u^k + \frac{\partial}{\partial y}E(\mathbf{u}^k)\frac{\partial v^{k+1/2}}{\partial y} + \frac{\partial}{\partial x}\eta(\mathbf{u}^k)\frac{\partial v^{k+1/2}}{\partial x} + \frac{\partial}{\partial y}\zeta(\mathbf{u}^k)\frac{\partial u^k}{\partial x} + \tau_y(\mathbf{u}^k), \tag{9}$$

where $E = \zeta + \eta$. The second level of the modified Euler time step is written as

$$m\frac{u^{k+1} - u^k}{\Delta t} = -C(\mathbf{u}^c)u^{k+1} + D(\mathbf{u}^c)v^c + \frac{\partial}{\partial x}E(\mathbf{u}^c)\frac{\partial u^{k+1}}{\partial x} + \frac{\partial}{\partial y}\eta(\mathbf{u}^c)\frac{\partial u^{k+1}}{\partial y} + \frac{\partial}{\partial x}\zeta(\mathbf{u}^c)\frac{\partial v^c}{\partial y} + \tau_x(\mathbf{u}^c) \tag{10}$$

$$m\frac{v^{k+1} - v^k}{\Delta t} = -C(\mathbf{u}^c)v^{k+1} - D(\mathbf{u}^c)u^c + \frac{\partial}{\partial y}E(\mathbf{u}^c)\frac{\partial v^{k+1}}{\partial y} + \frac{\partial}{\partial x}\eta(\mathbf{u}^c)\frac{\partial v^{k+1}}{\partial x} + \frac{\partial}{\partial y}\zeta(\mathbf{u}^c)\frac{\partial u^c}{\partial x} + \tau_y(\mathbf{u}^c), \tag{11}$$

where $\mathbf{u}^c = (\mathbf{u}^k + \mathbf{u}^{k+1/2})/2$, $u^c = (u^k + u^{k+1/2})/2$, and $v^c = (v^k + v^{k+1/2})/2$.

Note that (8)–(11) are semi-implicit equations because some of the terms in these equations are calculated using previously obtained ice velocity. Because of the semi-implicit treatment in the two-level modified Euler time stepping, the equations for the u and v components are effectively decoupled. These decoupled equations, (8)–(11), have better convergence properties and can be solved separately and efficiently following a LSR technique that utilizes an implicit tridiagonal matrix solver with the Thomas algorithm (see ZH). In addition to the two-level modified Euler time step, there is a third level of

correction in the LSR scheme which is designed to treat the Coriolis term and off-diagonal water drag term implicitly to ensure a stable solution for zero or small ice interaction. Since the third level of correction is not necessary for the new method to maintain numerical stability, it is not shown here.

2.3. New Method

As found by ZH, the LSR method converges rapidly and obtains a stable and true viscous-plastic solution for ice motion, if thus desired, with a few pseudo time steps. However, it requires an iterative LSR procedure, which is still computationally intensive as mentioned before. The new method presented here aims at eliminating the iterative procedure and therefore achieving a substantial improvement in computational efficiency. The method is essentially based on the same semi-implicit, two-level modified Euler time stepping scheme described above and by ZH. However, the LSR procedure is replaced by an alternating direction implicit (ADI) procedure, which has been widely used in numerically solving mathematical and engineering problems [see *Fletcher*, 1988]. Corresponding to (8)–(11), the new time stepping scheme is written as follows.

The first level of the modified Euler time step is

$$m\,\frac{u^{k+1*/2}-u^{k}}{\Delta t/2} = -C(\mathbf{u}^{k})u^{k+1*/2} + D(\mathbf{u}^{k})v^{k} + \frac{\partial}{\partial x}E(\mathbf{u}^{k})\,\frac{\partial u^{k+1*/2}}{\partial x} + \frac{\partial}{\partial y}\eta(\mathbf{u}^{k})\,\frac{\partial u^{k}}{\partial y} + \frac{\partial}{\partial x}\zeta(\mathbf{u}^{k})\,\frac{\partial v^{k}}{\partial y} + \tau_{x}(\mathbf{u}^{k}) \tag{12}$$

$$m\,\frac{u^{k+1/2}-u^{k+1*/2}}{\Delta t/2} = -C(\mathbf{u}^{k})u^{k+1/2} + D(\mathbf{u}^{k})v^{k} + \frac{\partial}{\partial x}E(\mathbf{u}^{k})\,\frac{\partial u^{k+1*/2}}{\partial x} + \frac{\partial}{\partial y}\eta(\mathbf{u}^{k})\,\frac{\partial u^{k+1/2}}{\partial y} + \frac{\partial}{\partial x}\zeta(\mathbf{u}^{k})\,\frac{\partial v^{k}}{\partial y} + \tau_{x}(\mathbf{u}^{k}) \tag{13}$$

for the u equation and

$$m\,\frac{v^{k+1*/2}-v^{k}}{\Delta t/2} = -C(\mathbf{u}^{k})v^{k+1*/2} - D(\mathbf{u}^{k})u^{k} + \frac{\partial}{\partial y}E(\mathbf{u}^{k})\,\frac{\partial v^{k+1*/2}}{\partial y} + \frac{\partial}{\partial x}\eta(\mathbf{u}^{k})\,\frac{\partial v^{k}}{\partial x} + \frac{\partial}{\partial y}\zeta(\mathbf{u}^{k})\,\frac{\partial u^{k}}{\partial x} + \tau_{y}(\mathbf{u}^{k}) \tag{14}$$

$$m\,\frac{v^{k+1/2}-v^{k+1*/2}}{\Delta t/2} = -C(\mathbf{u}^{k})v^{k+1/2} - D(\mathbf{u}^{k})u^{k} + \frac{\partial}{\partial y}E(\mathbf{u}^{k})\,\frac{\partial v^{k+1*/2}}{\partial y} + \frac{\partial}{\partial x}\eta(\mathbf{u}^{k})\,\frac{\partial v^{k+1/2}}{\partial x} + \frac{\partial}{\partial y}\zeta(\mathbf{u}^{k})\,\frac{\partial u^{k}}{\partial x} + \tau_{y}(\mathbf{u}^{k}) \tag{15}$$

for the v equation. The second level of the modified Euler time step is

$$m\,\frac{u^{k+1*}-u^{k}}{\Delta t/2} = -C(\mathbf{u}^{c})u^{k+1*} + D(\mathbf{u}^{c})v^{c} + \frac{\partial}{\partial x}E(\mathbf{u}^{c})\,\frac{\partial u^{k+1*}}{\partial x} + \frac{\partial}{\partial y}\eta(\mathbf{u}^{c})\,\frac{\partial u^{c}}{\partial y} + \frac{\partial}{\partial x}\zeta(\mathbf{u}^{c})\,\frac{\partial v^{c}}{\partial y} + \tau_{x}(\mathbf{u}^{c}) \tag{16}$$

$$m\,\frac{u^{k+1}-u^{k+1*}}{\Delta t/2} = -C(\mathbf{u}^{c})u^{k+1} + D(\mathbf{u}^{c})v^{c} + \frac{\partial}{\partial x}E(\mathbf{u}^{c})\,\frac{\partial u^{k+1*}}{\partial x} + \frac{\partial}{\partial y}\eta(\mathbf{u}^{c})\,\frac{\partial u^{k+1}}{\partial y} + \frac{\partial}{\partial x}\zeta(\mathbf{u}^{c})\,\frac{\partial v^{c}}{\partial y} + \tau_{x}(\mathbf{u}^{c}) \tag{17}$$

for the u equation and

$$m\,\frac{v^{k+1*}-v^{k}}{\Delta t/2} = -C(\mathbf{u}^{c})v^{k+1*} - D(\mathbf{u}^{c})u^{c} + \frac{\partial}{\partial y}E(\mathbf{u}^{c})\,\frac{\partial v^{k+1*}}{\partial y} + \frac{\partial}{\partial x}\eta(\mathbf{u}^{c})\,\frac{\partial v^{c}}{\partial x} + \frac{\partial}{\partial y}\zeta(\mathbf{u}^{c})\,\frac{\partial u^{c}}{\partial x} + \tau_{y}(\mathbf{u}^{c}) \tag{18}$$

$$m\,\frac{v^{k+1}-v^{k+1*}}{\Delta t/2} = -C(\mathbf{u}^{c})v^{k+1} - D(\mathbf{u}^{c})u^{c} + \frac{\partial}{\partial y}E(\mathbf{u}^{c})\,\frac{\partial v^{k+1*}}{\partial y} + \frac{\partial}{\partial x}\eta(\mathbf{u}^{c})\,\frac{\partial v^{k+1}}{\partial x} + \frac{\partial}{\partial y}\zeta(\mathbf{u}^{c})\,\frac{\partial u^{c}}{\partial x} + \tau_{y}(\mathbf{u}^{c}) \tag{19}$$

for the v equation.

Following the ADI procedure, we solve (12), (14), (16), and (18) row by row (in the x direction) and solve (13), (15), (17), and (19) column by column (in the y direction) using the implicit tridiagonal matrix solver with the Thomas algorithm. Note that this scheme does not involve the iterative LSR procedure, and each of the above eight equations is solved with one sweep of the matrix solver at each time step. However, if a true plastic solution is desired, the same procedure for pseudo time steps used by ZH can be applied to these equations. Generally, the solution is numerically stable, as shown in the appendix.

3. Simulation Results

How does the ADI method behave? We want to examine its numerical consistency and accuracy. In order to evaluate the ADI method in comparison with the LSR method we incorporated both schemes into two stand-alone sea ice models with different resolutions that cover the Arctic Ocean, the Barents Sea, and the Greenland-Iceland-Norwegian (GIN) Sea. Figure 1 shows the grid configuration of the sea ice model with 160-km resolution, and Figure 2 shows the grid configuration of the sea ice model with 40-km resolution. Both ice models, described in detail by *Zhang* [1993] and *Zhang et al*. [1998a], are two-category dynamic-thermodynamic models based on *Hibler*'s [1979] model. They are driven by surface forcing and ocean currents and heat flux. The daily surface forcing consists of geostrophic winds, surface air temperature, humidity, parameterized longwave and shortwave radiative fluxes [*Parkinson and Washington*, 1979], and precipitation. The geostrophic winds are calculated using sea level pressure fields determined by the International Arctic Buoy Program (IABP). The daily surface air temperature data are derived from buoys, manned drifting stations, and surrounding land stations [*Rigor et al*., 2000]. The precipitation is specified according to *Zhang et al*. [1998a] and used to calculate snow thickness in the model. The ocean currents and heat flux given by *Hibler and Zhang* [1993] are used to force the model.

To examine the numerical consistency and convergence of the ADI scheme, we conducted four series of test runs on an HP C180 workstation with a single processor. These test runs involve either the ADI scheme or the LSR scheme implemented in both the 160- and 40-km resolution ice models. All

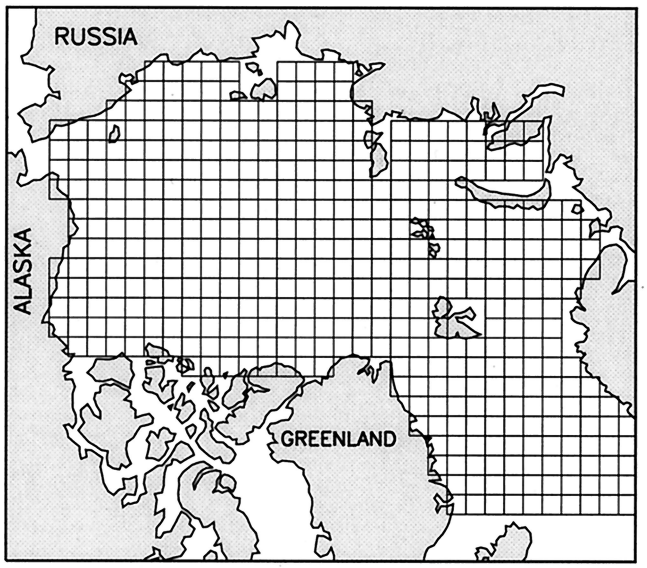

Figure 1. Grid configuration of the 160-km resolution sea ice model used for the Arctic Ocean and the Barents and Greenland-Iceland-Norwegian (GIN) Seas.

the models are integrated with decreasing time step intervals or varying pseudo time steps. Unless stated otherwise, the models are all driven by the daily forcing fields of 1996. Detailed information about the ice models and the model integrations are shown in Table 1. The model results are compared in sections 3.1–3.5.

3.1. Comparisons of Ice Internal Stress States

Figure 3 is a plot of ice internal stress states in principal stress space. With a 1-day time step and without pseudo time steps the stress states predicted by either the LSR method or the ADI method do not all lie on or within the elliptical yield curve (Figures 3a and 3d). They are scattered in a large area in the stress space. Thus, under such a time stepping condition without pseudo time steps the ice flow behavior predicted by the 160-km resolution ice model is not truly plastic. Given that the stress states are rather scattering, we expect that the ice deformation is somewhat randomly determined. When pseudo time steps are taken, however, the models start to approach a plastic solution, and the scattering of the stress states around the yield curve is reduced. With 5–15 pseudo time steps (Figures 3b, 3c, 3e, and 3f) the ice simulated by both methods is essentially in a state of fully viscous-plastic flow: Most of the stress states lie on the ellipse (plastic flow) and some fall inside the ellipse (viscous flow). This is desirable because the ice motion is described by the viscous-plastic rheology and, apparently, both numerical schemes are able to allow the ice to approach the state of the viscous-plastic flow.

However, a difference exists between the LSR solution and the ADI solution. As shown in Figure 3, the LSR scheme appears to obtain more stress states inside the ellipse, whereas

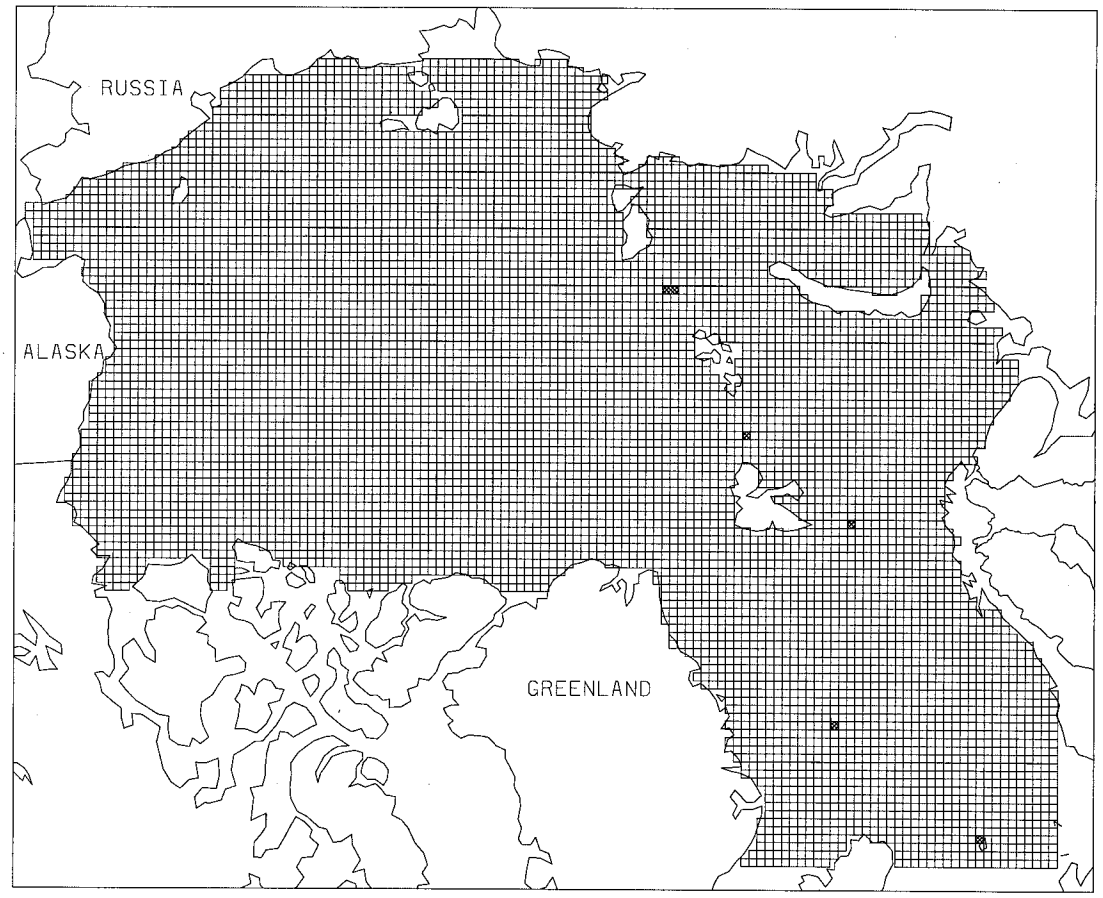

Figure 2. Grid configuration of the 40-km resolution sea ice model used for the Arctic Ocean and the Barents and GIN Seas. What appear as cells with crosses are islands.

Table 1. Description of the Sea Ice Models and Model Integrations

	Resolution, km	Grid Size	Time Step Interval, days	Pseudo Time Step	Numerical Method
Ice model 1	160	33×25	$1, \frac{1}{2}, \frac{1}{4}, \frac{1}{8}, \frac{1}{16}$	0, 5, 15	LSR, ADI
Ice model 2	40	130×102	$\frac{1}{4}, \frac{1}{8}, \frac{1}{16}, \frac{1}{32}$	0, 5, 15	LSR, ADI

LSR, line successive relaxation; ADI, alternating direction implicit.

the ADI scheme appears to obtain fewer stress states inside the ellipse. Given that both LSR and ADI schemes aim at solving the same mathematical problem described by the ice momentum equations, this raises a legitimate question: Why do the stress states predicted by the two methods look different? Note that the two methods represent different numerical approaches to solve the mathematical problem of high nonlinearity. Since numerical solutions are approximate solutions with varying degrees of accuracy (or inaccuracy), we do not expect that different numerical schemes would result in exactly the same solution with exactly the same accuracy. Nevertheless, we want to make sure that it is the numerical inaccuracy, not the numerical inconsistency, of the models that results in the different distributions of ice stress states as illustrated in Figure 3. Thus we conducted additional tests on the two methods with decreasing time step intervals (Table 1) in an effort to prove that the ADI method is numerically consistent and that it is the different numerical accuracies of the two methods that lead to the different distributions of ice stress states.

Figure 4 plots ice internal stress states from the same 160-km resolution ice model with a 1/16-day time step interval. With such a reduced time step interval both the LSR procedure and the ADI procedure approach a fully plastic solution even without pseudo time steps (Figures 4a and 4d). This means that for a sufficiently small time step, pseudo time steps are not necessary for both procedures to reach a truly plastic solution. In addition, with 5–15 pseudo time steps the ice stress states from the ADI method that fall inside the ellipse are comparable in quantity with those from the LSR method (Figures 4b, 4c, 4e, and 4f). This indicates that with a "sufficiently small" time step interval the ice stress states derived from the two different schemes are distributed in the stress space in the same manner. In other words, with decreasing time step intervals both procedures converge to the same solution of ice internal stress. This leads us to believe that the ADI method is numerically consistent.

3.2. Comparisons of Ice Velocity

In section 3.1 we have demonstrated that when the time step interval becomes smaller, both the ADI procedure and the LSR procedure converge to the same solution of ice internal stress. In this section, the behavior of the ADI solution of ice velocity is examined. To understand the overall behavior of the simulated ice velocity, a statistical analysis of ice velocity fields was carried out. Figure 5 shows the mean kinetic energy from both methods and mean velocity difference between both

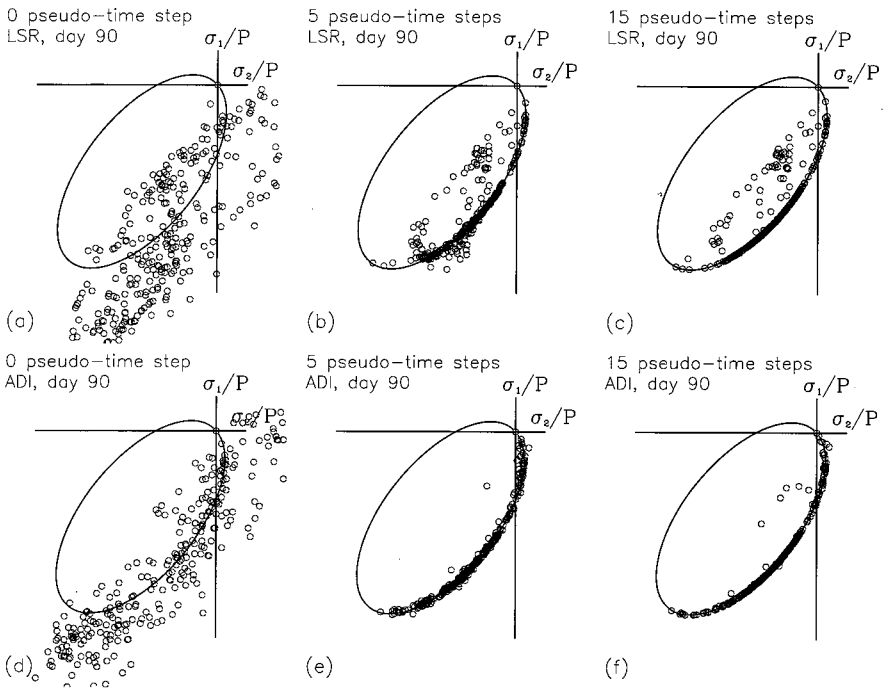

Figure 3. Principal ice internal stress states normalized by ice strength P predicted with and without pseudo time steps. The results are taken at day 90 (picked randomly) of 1996 from the 160-km resolution sea ice model with a 1-day time step interval (Table 1). The stress state at every ice point in the model domain is plotted.

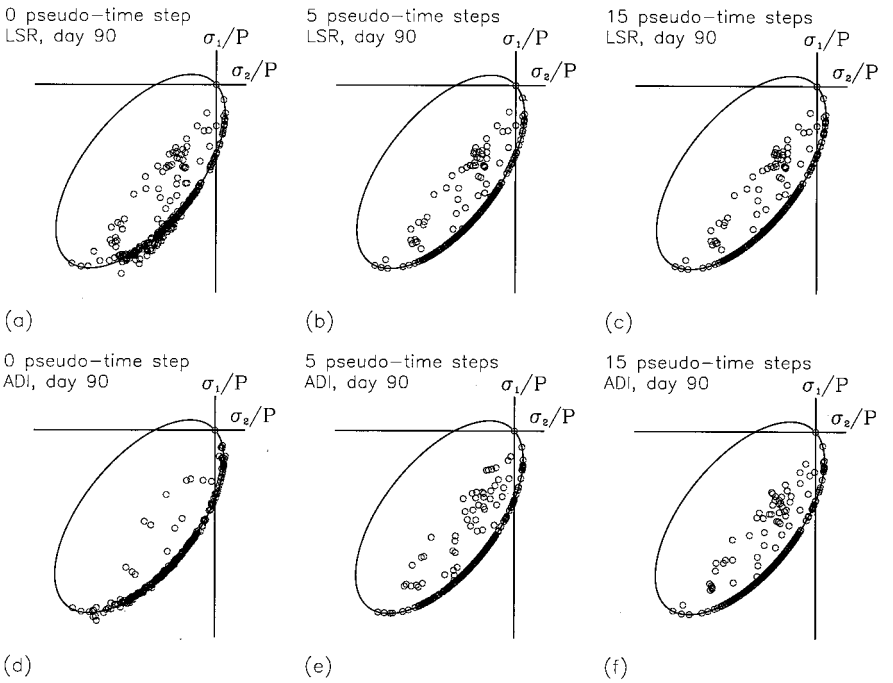

Figure 4. Principal ice internal stress states normalized by ice strength predicted with and without pseudo time steps. The results are taken at day 90 of 1996 from the 160-km resolution sea ice model with a 1/16 day time step. The stress state at every ice point in the model domain is plotted.

methods over 1-year integrations (1996) as a function of time step interval for both the 160- and 40-km resolution model configurations. The kinetic energy here is defined as the square of ice velocity at every grid cell with sea ice in the Arctic Basin, and the velocity difference is defined as the square of velocity difference between both methods. As shown in Figure 5, the kinetic energy values obtained using the different numerical schemes approach each other, and the velocity deviation diminishes as the time step interval decreases. Thus both the LSR method and the ADI method converge to the same solution of ice velocity with decreasing time step intervals on different model grid configurations of varying resolutions. This behavior is necessary for models to be numerically consistent and to be able to achieve higher accuracy with higher time resolution on a given model grid resolution.

Since both methods provide an approximation to a plastic solution via semi-implicit time stepping, neither method can be considered a priori to be better with a given model configuration. They approach the same and, presumably, the accurate solution of ice velocity with decreasing time step intervals. That is, they are equivalent as the time step interval approaches zero. However, they do differ in the way they approach the accurate solution. As shown in Figure 5, the ADI procedure generally overestimates the strength of ice motion when a crude time resolution is adopted. With the time step interval approaching zero the overestimation of ice speed is diminished, and the solution approaches the accurate one. In contrast, the LSR procedure generally underestimates ice speed with a crude time resolution and approaches the accurate solution with an increasing ice speed as the integration time step interval approaches zero. These contrasting behaviors of the two different procedures remain with or without pseudo time steps. With pseudo time steps, however, both procedures approach the accurate solution faster.

Note that the accurate solution of kinetic energy from the 40-km resolution model with a 1/16-day time step is slightly larger than that from the 160-km resolution model with a 1/32-day time step. This is because the former is calculated using ice velocity averaged over a smaller area (40×40 km^2) and the latter is averaged over a larger area (160×160 km^2). However, the difference between the two accurate solutions is small. This indicates that the models converge to the same accurate solution with increasing model resolutions, which is another aspect of numerical consistency.

Why does the ADI method overestimate the ice motion and the LSR method underestimate the ice motion when a crude time resolution is used? We may not be able to pinpoint the exact cause because it is numerical not physical. However, the answer appears to be linked to the behavior of the simulated ice internal stress shown in Figures 3 and 4. With a crude time resolution the ADI procedure tends to overestimate the plastic state of ice (more stress points on the yield curve), which leads to stronger ice motion, and with a crude time step the LSR procedure tends to overestimate the viscous state of ice (more stress points inside the yield curve), which leads to weaker ice motion.

The difference in ice velocity between the ADI and LSR methods is further illustrated in Figure 6, which plots the annual mean ice velocity fields and the corresponding difference fields for the 160-km resolution sea ice model integrated with two different time step intervals. With a 1-day time step interval the velocity difference between the two schemes is relatively large; the difference can be as large as 0.5 cm s^{-1} (Figure 6e). This is because with such a time resolution the ADI procedure overestimates the ice speed and the LSR procedure underestimates the ice speed, as mentioned before. With a 1/16-day time step interval, however, the difference becomes rather small (Figure 6f). Most of the velocity vector

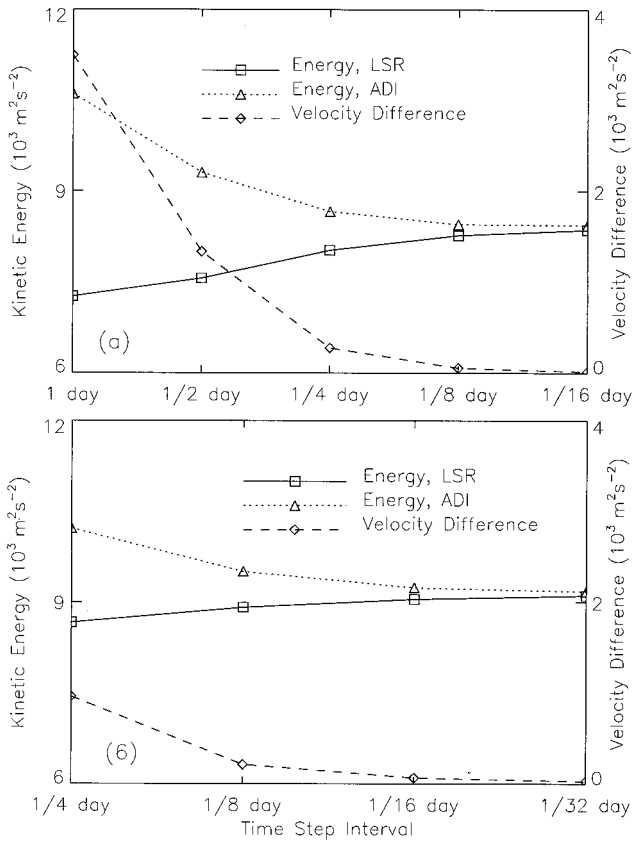

Figure 5. Mean kinetic energy and velocity difference versus time step interval from (a) the 160-km resolution sea ice model and (b) the 40-km resolution sea ice model using 5 pseudo time steps. The solid line is for $\Sigma_N \Sigma_M \mathbf{U}^2_{\mathrm{LSR}}/(NM)$, the dotted line is for $\Sigma_N \Sigma_M \mathbf{U}^2_{\mathrm{ADI}}/(NM)$, and the dashed line is for $\Sigma_N \Sigma_M (\mathbf{U}_{\mathrm{ADI}} - \mathbf{U}_{\mathrm{LSR}})^2/(NM)$ (velocity difference). Here M is the number of total grid points with ice in the Arctic Basin, and N is the number of total time steps in 1-year integration.

differences are zero. The maximum velocity vector difference among all the grid cells is <1 mm s^{-1} in magnitude. This behavior is also basically true with the results from the 40-km resolution sea ice model, as shown in Figure 7. All these indicate once again that both the ADI scheme and the LSR scheme converge to the same solution of ice velocity as the time step interval decreases.

Finally, it is worth mentioning that both the ADI and LSR methods are based on solving the ice momentum equations with the u and v component equations decoupled (ZH). The errors with large time step intervals shown in Figures 5–7 are certainly related to the models' crude resolutions in time. They may also be related to the effect of decoupling the equations. Decreasing time step intervals not only reduces the numerical errors due to a crude time resolution but also strengthens the coupling of the equations since they exchange information more often.

3.3. Comparisons of the Simulated Ice Motion and Buoy Motion

As demonstrated earlier, both the ADI solution and the LSR solution converge to the same, accurate solution with a sufficiently small time step interval on a given model grid. Otherwise, the LSR method tends to underestimate the ice speed and the ADI method tends to overestimate the ice speed. The question is, What time step interval should one select? Of course, the smaller the time step interval is, the more accurate solution one obtains. In practice, however, considerations are given on the basis of a balance between computational cost and numerical accuracy in selecting an appropriate integration time step interval. Because of the constraints of computer resources, using very small time steps to integrate the sea ice model is often impractical, particularly in long-term climate studies. In fact, in order to reduce computational cost it is often the numerical stability criterion that is used to determine the time step interval. That is, the time step interval is selected to be as large as possible unless it is out of the range of numerical stability. As a result, the selected integration time step interval often may not be deemed sufficiently small. Then the question is, What are the consequences of integrating a certain numerical model with a relatively crude time resolution on a given model grid configuration? This is an issue of numerical accuracy that has rarely been addressed before. If the model integration is numerically stable, sea ice modelers often tend to accept the model output as is, without considering its numerical accuracy.

In this and the following sections we want to address this issue by examining the model outputs from both the ADI and the LSR schemes without a sufficiently small time step of integration. We hope to obtain some idea of how the numerical inaccuracy resulting from a crude time resolution affects the results of different numerical models. For this purpose we run the 40-km resolution sea ice model from 1979 to 1996 using the surface forcing described earlier. The ice model is integrated using a 1/4-day time step and five pseudo time steps with these two numerical schemes. The simulated ice velocity results are then compared with Arctic buoy data in this section. Comparisons of ice thicknesses and concentrations are made in section 3.4.

Figure 8 compares the distributions of the simulated ice speed and buoy drift speed. A conspicuous feature shown in Figure 8 is a substantial overprediction of ice stoppage by the LSR method (see the large peak at the origin), which is attributed to its tendency to underestimate ice speed. In contrast, the ADI method underpredicts, to a lesser degree, ice stoppage, which is attributed to its tendency to overestimate ice speed.

Making use of the results in Figure 8, we found that, overall, in 1981–1987 the Arctic buoys have a mean drift speed of 0.075 m s^{-1}. The simulated mean ice motion, driven by the particular wind forcing, is 0.070 m s^{-1} for the LSR method and 0.081 m s^{-1} for the ADI method. Thus, statistically, the ice simulated by the ADI procedure moves ~8% faster than the observed drift, while that simulated by the LSR procedure moves ~7% slower. Of the two procedures, the ice simulated by the ADI procedure moves ~15% faster than that simulated by the LSR procedure. Thus an uncertainty or bias of up to ~10% is likely with a numerical model of crude time resolution. Note, however, that using different wind forcing or different wind and water drag coefficients would give different statistical values. Nevertheless, these statistical results and Figure 8 illustrate the different behaviors of these two numerical methods when they do not converge to the same, accurate solution.

3.4. Comparisons of Ice Thickness and Concentration

That both the ADI method and the LSR method converge to the same solution of ice velocity with a sufficiently small

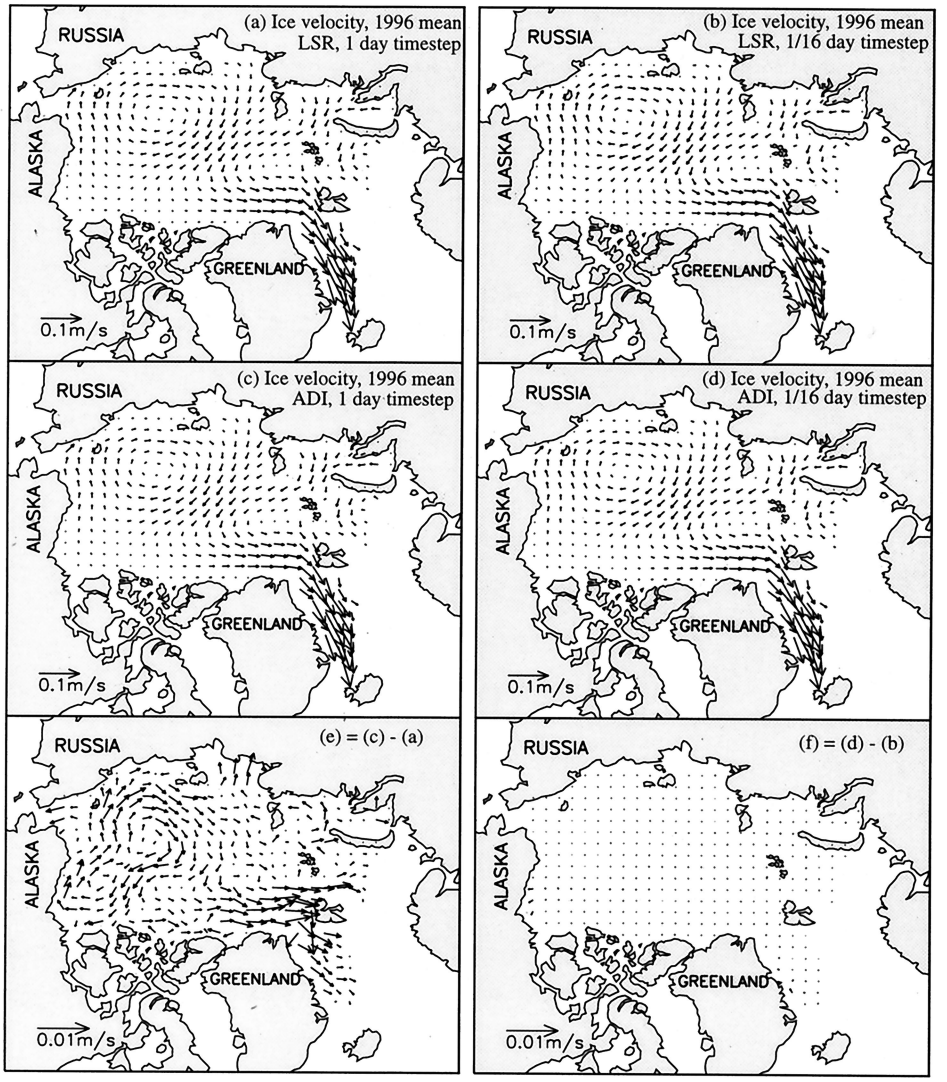

Figure 6. Annual (1996) mean fields of ice velocity and velocity difference between the alternating direction implicit (ADI) method and the line successive relaxation (LSR) method predicted by the 160-km resolution sea ice model. Note the different vector scales in different plots.

time step interval implies that both methods converge to the same solution of ice thermodynamics under a given thermal forcing. When a relatively crude time resolution is used, however, we expect that the simulated ice thickness and concentration would behave differently with the two different methods because the simulated ice velocity behaves differently. To obtain an idea of how the spatial distributions of ice thickness predicted by the two methods, with a large time step interval, differ from each other, we plotted the 1987 and 1996 mean ice thickness fields and the corresponding differences (Figure 9). We picked 1987 and 1996 because the anticyclonic wind circulation in the Arctic is strong in 1987 and weak in 1996. In general, both methods predict thicker ice along the Canadian Archipelago and North Greenland coast and thinner ice in the eastern Arctic, which generally, is in agreement with the pattern observed by *Bourke and Garrett* [1987]. This pattern is, however, subject to significant interannual variations, as illustrated by the different thickness distributions in 1987 and 1996 induced by different wind and thermodynamic forcing fields.

Although the thickness distribution patterns created by both methods are basically similar, there are some significant differences. The ADI method generally predicts thinner ice within the Arctic Ocean and slightly thicker ice in some areas of the marginal ice zone in the Barents and Greenland Seas. In the Arctic Ocean the seasonally varying mean ice thickness calculated by the ADI scheme is always smaller than that calculated by the LSR scheme, as shown in Figures 10a and 10b. However, the difference varies from season to season. The difference is largest in summer when the ice in the Arctic is thinner in general and is smallest in late winter and early spring (April and May) when the ice is thicker. In fact, the seasonally varying difference in ice thickness is negatively well correlated with the mean thickness. In other words, when the Arctic ice becomes thicker, the difference in ice thickness predicted by the ADI procedure and the LSR procedure becomes smaller, and vice versa. This means that the ADI method tends to predict more seasonal variations in ice thickness.

Similar to ice thickness, ice concentration predicted by the ADI method is also always smaller than that predicted by the LSR method (see Figures 10c and 10d) when a 1/4-day time

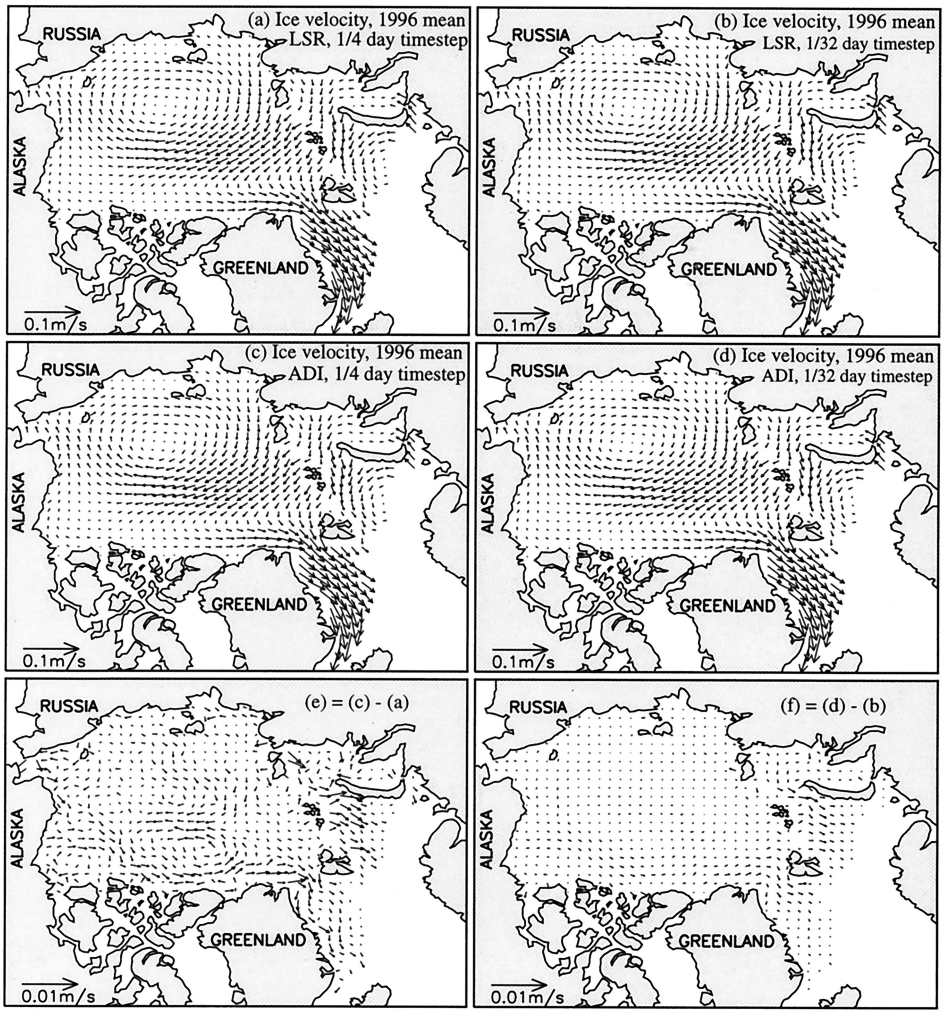

Figure 7. Annual (1996) mean fields of ice velocity and velocity difference between the ADI method and the LSR method predicted by the 40-km resolution sea ice model. One vector is drawn for every nine grid cells. Note the different vector scales in different plots.

step interval is used to integrate the models, particularly in summer (see Figures 10c and 10d). Again, the difference is negatively well correlated with the mean concentration. Thus the ADI method tends to predict more seasonal variability in ice concentration as well.

Why does the ADI method predict less ice in the Arctic Ocean and more ice in the marginal ice zone than the LSR method? The answer lies in the stronger ice motion simulated by the ADI method. By simulating stronger ice motion the ADI method exports more ice via Fram Strait, thus resulting in less ice in the Arctic and more ice in the marginal ice zone in the Barents and GIN Seas. Figure 11 shows annual mean areal and volume ice exports at Fram Strait. Both the areal and the volume outflows show pronounced interannual variability. The ADI method consistently predicts greater areal and volumetric outflows than the LSR method. However, the difference in areal outflow is relatively steady from year to year, whereas the difference in volume outflow changes considerably, owing to interannual variations in ice thickness in the Fram Strait area. Note that, in most of the years, the areal outflow predicted by the ADI procedure appears to be slightly closer to the observational estimate of *Kwok and Rothrock* [1999]. However, since the ADI scheme tends to overestimate ice motion, the outflow calculated using it may still be overestimated under the given wind forcing. In contrast, the outflow calculated by the LSR method may be underestimated under the same wind forcing because of its tendency to underestimate ice motion.

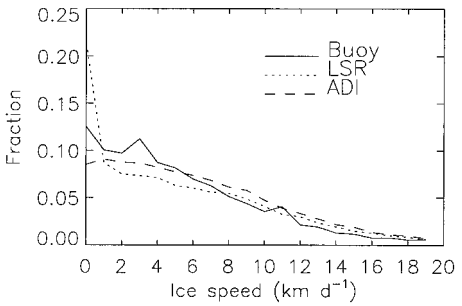

Figure 8. Distributions of simulated ice speed and observed Arctic buoy drift speed, based on all the available daily buoy drift data for the Arctic from 1981 to 1987 and simulated daily mean ice velocities corresponding to the buoy data.

Since the ADI method drives more ice out of the Arctic

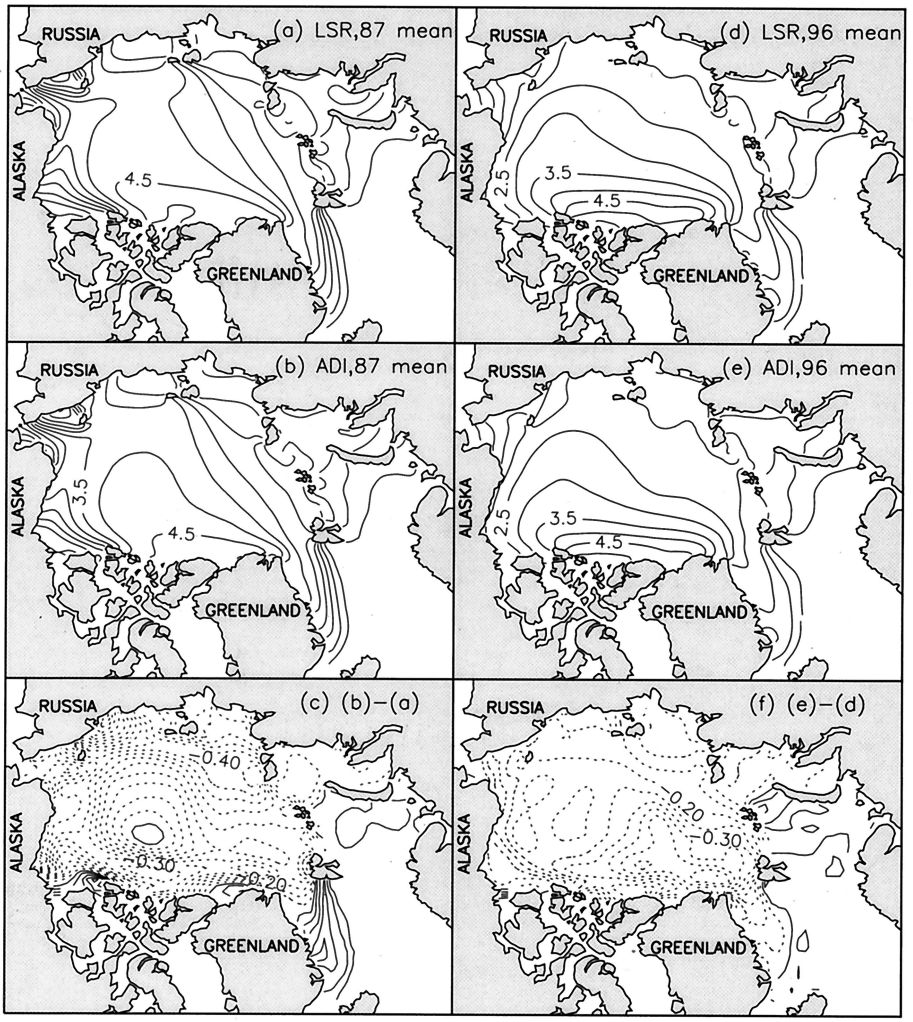

Figure 9. Annual mean ice thickness fields for 1987 and 1996 (Figures 8a, 8b, 8d, and 8e). Figure 8c gives ice thickness field in Figure 8b minus that in Figure 8a. Figure 8f gives ice thickness field in Figure 8e minus that in Figure 8d. Contour interval is 0.5 m in Figures 8a, 8b, 8d, and 8e and 0.05 m in Figures 8c and 8f. Solid lines are positive; dotted lines are negative.

Ocean each year, the mean total Arctic ice volume calculated by the ADI method is always less than that calculated by the LSR method, as shown in Figure 12a. Note that there is almost no difference in the total ice volume predicted in 1979 because both model integrations start at the same initial conditions after integrating 1979 for four times using the LSR method. After an initial increase during the first 3 years, the difference in total ice volume becomes quite steady from year to year. Figure 12b shows passive microwave satellite observations of mean ice concentration averaged over the Arctic, and simulation results. As reported by previous investigations [*Johannessen et al*., 1995; *Gloersen and Campbell*, 1991], the observations show a slight but noticeable downward trend in the extent of the Arctic ice in recent years, which is more or less captured by both methods. Compared to the observations, both methods overpredict ice concentration by a few percent. Again, the ADI method computes less ice concentration, which is slightly closer to the observations. Nevertheless, the ADI method may still underestimate the ice concentration with the given thermodynamical forcing because of its tendency to overestimate ice outflow when a crude integration time step is adopted.

3.5. Comparisons of Computational Efficiency

One of the major differences between the way the two methods numerically solve the ice momentum equations is that the LSR procedure requires an iterative solution, whereas the ADI procedure requires a direct solution. Since the direct solution does not involve recursive iterations, the ADI method is more efficient than the LSR method with or without pseudo time steps. With a single-processor workstation, a 1-year integration takes 3266 s of CPU time for the LSR procedure to solve the momentum equations without pseudo time steps, whereas the ADI procedure only takes 182 s (Table 2). That is, the ADI procedure is ~18 times faster than the LSR procedure when no pseudo time steps are used. If a fully plastic solution is desired and 15 pseudo time steps are taken at each physical time step, 7784 and 1007 s of CPU time are needed for the LSR and the ADI procedures, respectively, to do a 1-year integration. Obviously, the speed advantage of the ADI method over the LSR method is reduced with 15 pseudo time steps because the LSR procedure generally needs fewer iterations to converge in pseudo time steps. The speed advantage of

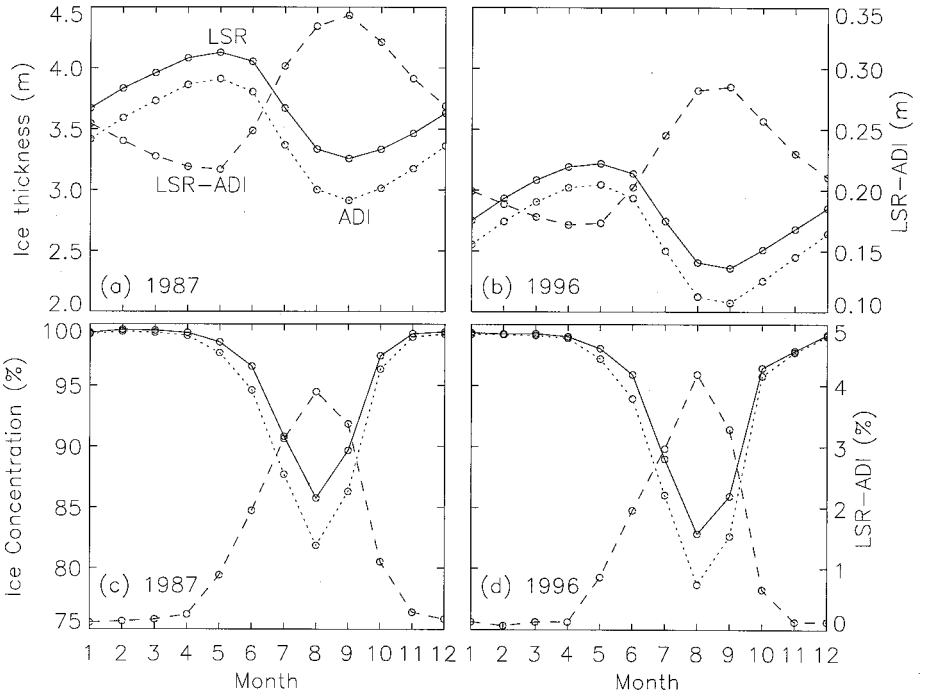

Figure 10. Monthly mean ice thickness in the Arctic Ocean predicted by the LSR and ADI methods and the difference between them for (a) 1987 and (b) 1996; monthly mean ice concentration in the Arctic Ocean predicted by the LSR and ADI methods and their difference for (c) 1987 and (d) 1996.

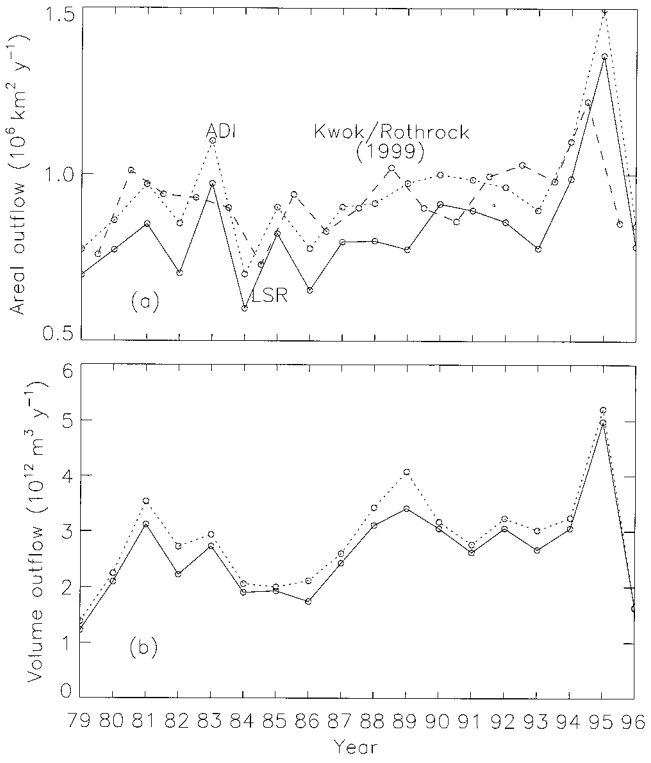

Figure 11. Simulated annual mean ice outflows at Fram Strait. (a) Areal outflow and (b) volume outflow. The results from *Kwok and Rothrock* [1999] based on satellite observations are included.

the ADI method would also be reduced with small time step intervals. Still, using the ADI procedure saves CPU time. When using a machine with parallel processors, we speculate that there would be even greater savings in CPU time. This is based on the fact that there is no data dependency with the ADI scheme's outer loop of the matrix solver and therefore the outer loop should be easily adapted to parallel computing. However, tests are needed to assess the performance of the ADI procedure on a massively parallel machine.

4. Concluding Remarks

The thrust of this work was to develop a numerical model for sea ice dynamics that is computationally efficient and numerically consistent. Specifically, the goal was to achieve high efficiency while still keeping the physics of the ice rheology intact. By eliminating the iterative LSR procedure adopted in the ZH method and replacing it with an ADI procedure that goal appears to have been achieved.

Being computationally efficient, the ADI procedure produces a direct solution of the sea ice momentum equations without recursive iterations, which yields an enormous savings in CPU time. Specifically, the new ADI method is ~18 times faster than the LSR method without pseudo time steps and 8 times faster with 15 pseudo time steps when run on a workstation. If a coarse time step interval is used, we recommend using 5–15 pseudo time steps for general large-scale modeling studies to provide a reasonable approximation to plastic flow. Pseudo time stepping, however, is an iterative procedure. With more pseudo time steps, the advantage of the ADI solution in efficiency over the LSR solution is reduced (Table 2). Nevertheless, increasing pseudo time steps is desirable if computer resources permit since more pseudo time steps are likely to achieve a better plastic solution.

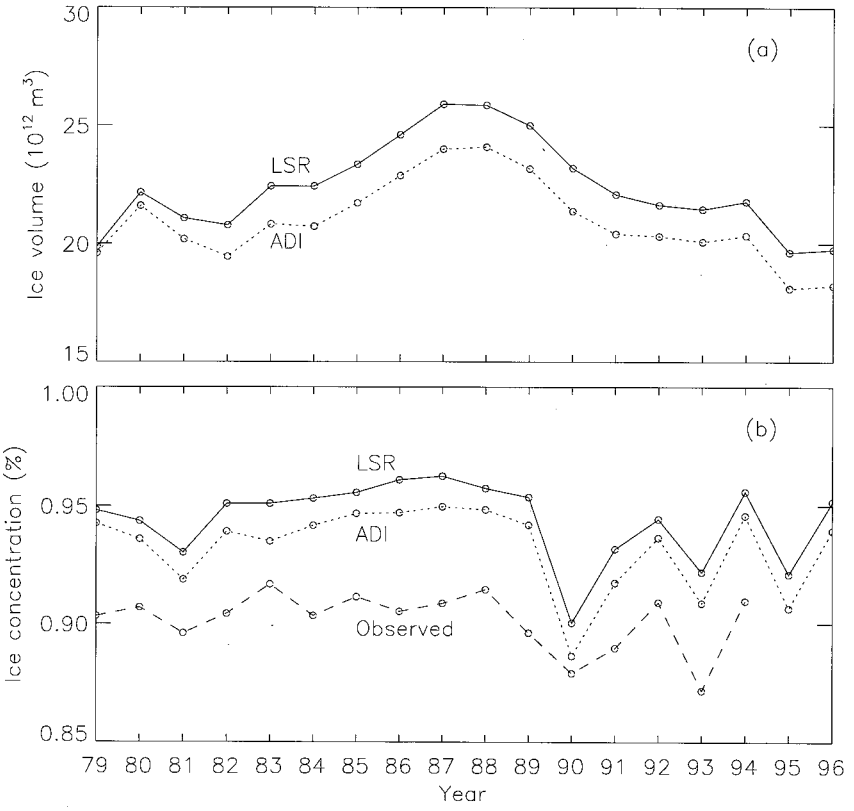

Figure 12. (a) Simulated annual mean total ice volume in the Arctic Ocean. (b) Annual mean ice concentration in the Arctic simulated by the models and observed by satellites (the Satellite Multichannel Microwave Radiometer and the Special Sensor Microwave/Imager).

With the ADI method the CPU time consumed in computing ice dynamics is generally less than that consumed in computing ice thermodynamics even with a two-category ice model. This suggests that if the ADI method is employed for calculating ice dynamics, any continuing effort to improve the efficiency of ice models as a whole should be more or less directed to computations of thermodynamics and other components of ice models, particularly in the case of multicategory thickness distribution sea ice models that lean heavily on computations of thermodynamic growth and mechanical ridging.

Like the LSR method, the ADI method is able to approach a viscous plastic solution as designed by the viscous plastic rheology. At a coarse time resolution both the ADI method and the LSR method need a few pseudo time steps to reach a viscous-plastic solution. Such a solution may not be an accurate solution. However, with a sufficiently small time step interval an accurate viscous-plastic solution is obtained by either method with or without pseudo time steps (although pseudo time steps help to accelerate the convergence). In other words, with decreasing time step intervals both the ADI method and the LSR method converge to the same, accurate viscous-plastic solution for a given model grid configuration and surface forcing. This proves that the ADI procedure is numerically consistent and is able to achieve a higher accuracy with a higher model resolution in time.

Table 2. CPU Time Required for the 40-km Resolution Ice Model to Reach a Plastic Solution for Ice Motion When Using Pseudo Time Stepping for a 1-Year Integration on an HP C180 Workstation

Pseudo Time Steps	LSR, s	ADI, s	LSR/ADI, s
0	3266	182	17.9
5	6364	468	13.6
15	7784	1007	7.7

The ADI method's ability to efficiently approach an accurate viscous-plastic solution is not only important in simulating ice motion but also important in predicting oriented leads, cracks, and ridges of sea ice. As pointed out by *Hibler and Schulson* [1997], the occurrence and orientation of leads/ridges depend on the conditions of ice stresses, such as where the stress states are located in principal stress space. The ice stress conditions in turn depend on the accuracy of the viscous-plastic solution. An accurate viscous-plastic solution with ice stress states either on the plastic yield curve or inside the yield curve, such as shown in Figure 4, would provide useful information to estimate the formation of leads/ridges. If the solution is such as shown in Figures 3a and 3d, however, meaningful prediction of leads/ridges would be impossible.

The issue of numerical inaccuracy resulting from coarse model time resolutions is addressed. The results indicate that either the ADI method or the LSR method is likely to create a significant bias, up to 10% or more, in the solution if a sufficiently small time step interval is not used. With a coarse time stepping, the ADI method tends to overestimate ice motion. The overestimation of ice motion results in a slight un-

derestimation of ice stoppage compared to the Arctic buoy data and an increase in both areal and volume ice exports via Fram Strait compared to the results of the LSR method, which often leads to an ice cover that is thinner in the Arctic Ocean and thicker in the marginal ice zone in the Barents and Greenland seas. The behaviors of the LSR method are just the opposite. Thus, in numerical investigations of sea ice we need to use appropriate model time step intervals in order to reduce, as much as possible, numerically induced bias. From Figure 5 we suggest using time step intervals $\leq$ 1/4 and a 1/8 day for sea ice models with 160-km and 40-km resolutions, respectively. We do not intend, however, to make a general recommendation for selecting model time step intervals for individual model applications. We only recommend that for each individual model application it is useful to perform an accuracy analysis similar to that made for Figure 5. By examining the asymptotic behavior of the solution as the time step interval decreases, we should be able to select a time step interval that satisfies our needs for numerical accuracy as well as modeling economy.

Appendix: Stability Analysis Using the Von Neumann Method

Following the approach used in Appendix A of ZH, we consider a special case of the ice momentum equations to demonstrate the stability behavior of the time stepping procedure used with the ADI method. In this special case the shear and bulk viscosities, the water drag coefficient, and the Coriolis term are taken to be spatially constant. With these simplifications and without τ_x and τ_y the momentum equations, (6) and (7), become

$$m\frac{\partial u}{\partial t} = -Cu + Dv + E\frac{\partial^2 u}{\partial x^2} + \eta\frac{\partial^2 u}{\partial y^2} + \zeta\frac{\partial^2 v}{\partial x \partial y} \tag{20}$$

$$m\frac{\partial v}{\partial t} = -Cv - Du + E\frac{\partial^2 v}{\partial y^2} + \eta\frac{\partial^2 v}{\partial x^2} + \zeta\frac{\partial^2 u}{\partial x \partial y}. \tag{21}$$

The stability analysis is based on the concept that a particular numerical method is stable if the cumulative effect of all the round-off errors produced in the application of the method is small. Following Von Neumann's method [*Fletcher*, 1988], we assume the errors for ice velocities u and v at time step k and grid cell (i, j) are, respectively,

$$\gamma_{ij}^k = u_{ij}^k - u_{ij}^{k^*} = G^k e^{I(\alpha i + \beta j)} \tag{22}$$

$$\varepsilon_{ij}^k = v_{ij}^k - v_{ij}^{k^*} = H^k e^{I(\alpha i + \beta j)}, \tag{23}$$

where $u_{ij}^{k^*}$ and $v_{ij}^{k^*}$ are true solutions, u_{ij}^k and v_{ij}^k are approximations, and $I = \sqrt{-1}$.

As a first step, we examine the stability of the first level of the modified Euler time step. By applying (22) and (23) to (20) and using the time stepping scheme in (12) and (13) the following expressions can be derived:

$$\left(\frac{2m}{\Delta t} + C + \frac{4E\sin^2\frac{\alpha}{2}}{h^2}\right)\gamma_{ij}^{k+1/2^*} = \left(\frac{2m}{\Delta t} - \frac{4\eta\sin^2\frac{\beta}{2}}{k^2}\right)\gamma_{ij}^k + \left(D + \frac{\zeta\sin\alpha\sin\beta}{hk}\right)\varepsilon_{ij}^k \tag{24}$$

$$\left(\frac{2m}{\Delta t} + C + \frac{4\eta\sin^2\frac{\beta}{2}}{k^2}\right)\gamma_{ij}^{k+1/2} = \left(\frac{2m}{\Delta t} - \frac{4E\sin^2\frac{\alpha}{2}}{h^2}\right)\gamma_{ij}^{k+1/2^*} + \left(D + \frac{\zeta\sin\alpha\sin\beta}{hk}\right)\varepsilon_{ij}^k, \tag{25}$$

where $h = \Delta x$ and $k = \Delta y$. For further simplicity, assume the error in u is equivalent in magnitude to that in v, such that $\varepsilon_{ij}^k \cong \gamma_{ij}^k$; then combining (24) and (25) leads to

$$\begin{aligned}\gamma_{ij}^{k+1/2} = &\left[\left(a^2 - \frac{4aE\sin^2\frac{\alpha}{2}}{h^2} - \frac{4a\eta\sin^2\frac{\beta}{2}}{k^2} + \frac{16E\eta\sin^2\frac{\alpha}{2}\sin^2\frac{\beta}{2}}{h^2k^2} + \frac{(a+b)\zeta\sin\alpha\sin\beta}{hk}\right)\right.\\ &\cdot\left.\left(b^2 + \frac{4bE\sin^2\frac{\alpha}{2}}{h^2} + \frac{4b\eta\sin^2\frac{\beta}{2}}{k^2} + \frac{16E\eta\sin^2\frac{\alpha}{2}\sin^2\frac{\beta}{2}}{h^2k^2}\right)^{-1}\right]\gamma_{ij}^k\\ = &\, G'\gamma_{ij}^k,\end{aligned} \tag{26}$$

where $a = 2m/\Delta t + D$, $b = 2m/\Delta t + C$, and G' is the coefficient before γ_{ij}^k.

For the numerical scheme to be stable at the first level of the modified Euler time stepping, G' must be $\leq$1. In order to evaluate G' it is useful to first evaluate C and D. In most of the ice models based on *Hibler*'s [1979] model, C and D are set such that $C \geq 0.25\cos(25°) = 0.23$ kg s^{-1} and, correspondingly, $D - mf \geq 0.25\sin(25°) = 0.11$ kg s^{-1}. Since $|f| < 1.5 \times 10^{-4}$ s^{-1}, the ice has to be $\sim$1 m thick for D to be larger than C (see section 2.1). Keeping this in mind, we then proceed with further analysis.

First, consider a special case in which there is no ice or the ice is so thin that the ice mass and ice stress are negligibly small. Thus $G' \cong D^2/C^2 = 0.11^2/0.23^2 \leq 1$. Now consider a more general case in which the ice is <1 m thick. In this case, $D \leq C$ and, therefore $a \leq b$. In order for $G' \leq 1$ the following inequality, which is derived by applying (5) and assuming $h = k$ for further simplicity, has to be satisfied:

$$-4a(1+e^2)\sin^2\frac{\alpha}{2} - 4a\sin^2\frac{\beta}{2} + (a+b)e^2\sin\alpha\sin\beta \leq 4b(1+e^2)\sin^2\frac{\alpha}{2} + 4b\sin^2\frac{\beta}{2}. \tag{27}$$

Numerically evaluating the terms in (27), we found that for $0 \leq b/a \leq 10$ and $0° \leq \alpha, \beta < 360°$, (27) is indeed satisfied. This indicates that for $1 \leq b/a \leq 10$ and an ice thickness <1 m, $G' \leq 1$.

Finally, consider the case in which the ice is about or more than 1 m thick. Under such a condition, $a \geq b$. However, the shear and bulk viscosities become so large [*Hibler*, 1979] that the terms a^2 and b^2 in G' are small compared to the other terms unless α and β are both zero at the same time. Consequently, (27) is still useful in judging the stability properties for

this case. This means that for $0 \leq b/a \leq 1$ and α and β not being zero at the same time, $G' \leq 1$.

A similar outcome can be obtained if this analysis procedure is applied to (14) and (15), (16) and (17), and (18) and (19). Therefore, we conclude that generally, the ADI method is numerically stable if α and β are not zero simultaneously, although a series of assumptions has been made in the course of the stability analysis.

Acknowledgments. We thank W. D. Hibler III and M. Steele for helpful discussions, R. S. Pritchard and two anonymous reviewers for their constructive comments, I. Rigor for providing IABP sea level pressure and surface air temperature data, D. Thomas for providing satellite ice concentration data, and A. Schweiger and M. Ortmeyer for computer assistance. This work was supported by an EOS Interdisciplinary Investigation, Polar Exchange at the Sea surface (POLES) under NASA grant NAGS-4375.

References

Bourke, R. H., and R. P. Garrett, Sea ice thickness distribution in the Arctic Ocean, *Cold Reg. Sci. Technol*., *13*, 259–280, 1987.

Coon, M. D., Mechanical behavior of compacted Arctic ice floes, *JPT J. Pet. Technol*., *26*, 466–470, 1974.

Fletcher, C. A. J., *Computational Techniques for Fluid Dynamics*, vol. 1, 409 pp., Springer-Verlag, New York, 1988.

Geiger, C. A., W. D. Hibler III, and S. F. Ackley, Large-scale sea ice drift and deformation: Comparison between models and observations in the western Weddell Sea during 1992, *J. Geophys. Res*., *103*, 21,893–21,913, 1998.

Gloersen, P., and W. J. Campbell, Recent variations in Arctic and Antarctic sea-ice covers, *Nature*, *352*, 33–36, 1991.

Hibler, W. D., III, A dynamic thermodynamic sea ice model, *J. Phys. Oceanogr*., *9*, 815–846, 1979.

Hibler, W. D., III, and C. F. Ip, The effect of sea ice rheology on Arctic buoy drift, in *Ice Mechanics 1995*, *AMD*, vol. 207, edited by J. P. Dempsey and Y. D. S. Rajapakse, pp. 255–264, Am. Soc. of Mech. Eng., New York, 1995.

Hibler, W. D., III, and E. M. Schulson, On modeling sea-ice fracture and flow in numerical investigations of climate, *Ann. Glaciol*., *25*, 26–32, 1997.

Hibler, W. D., III, and J. Zhang, Interannual and climatic characteristics of an ice-ocean circulation model, Advanced Research Workshop on Ice and Climate, N. Atl. Treaty Org., Aussois, France, 1993.

Ip, C. F., Numerical investigation of different rheologies on sea-ice dynamics, Ph.D. thesis, 242 pp., Dartmouth College, Hanover, N. H., 1993.

Ip, C. F., W. D. Hibler III, and G. M. Flato, On the effect of rheology on seasonal sea-ice simulations, *Ann. Glaciol*., *15*, 17–25, 1991.

Johannessen, O. M., M. Miles, and E. Bjorgo, The Arctic's shrinking sea ice, *Nature*, *376*, 126–127, 1995.

Kwok, R., and D. A. Rothrock, Variability of Fram Strait flux and North Atlantic Oscillation, *J. Geophys. Res*., *104*, 5177–5189, 1999.

McPhee, M. G., The upper ocean, in *The Geophysics of Sea Ice*, edited by N. Untersteiner, pp. 339–394, Plenum, New York, 1986.

Parkinson, C. L., and W. M. Washington, A large-scale numerical model of sea ice, *J. Geophys. Res*., *84*, 311–337, 1979.

Pritchard, R. S., An elastic-plastic constitutive law for sea ice, *J. Appl. Mech*., *42E*, 379–384, 1975.

Rigor, I. G., R. L. Colony, and S. Martin, Variations in surface air temperature observations in the Arctic, 1979–1997, *J. Clim*., in press, 2000.

Song, X., Numerical investigation of a viscous plastic sea-ice forecasting model, M.S. thesis, 108 pp., Dartmouth College, Hanover, N. H., 1994.

Zhang, J., A high resolution ice-ocean model with imbedded mixed later. Ph.D. thesis, 229 pp., Dartmouth College, Hanover, N. H., 1993.

Zhang, J., and W. D. Hibler III, On an efficient numerical method for modeling sea ice dynamics, *J. Geophys. Res*., *102*, 8691–8702, 1997.

Zhang, J., W. D. Hibler III, M. Steele, and D. A. Rothrock, Arctic ice-ocean modeling with and without climate restoring, *J. Phys. Oceanogr*., *28*, 191–217, 1998a.

Zhang, J., D. A. Rothrock, and M. Steele, Warming of the Arctic Ocean by a strengthened Atlantic inflow: Model results, *Geophys. Res. Lett*., *25*, 1745–1748, 1998b.

Zhang, Y., W. Maslowski, and A. J. Semtner, Impact of mesoscale ocean currents on sea ice in high-resolution Arctic ice and ocean simulations, *J. Geophys. Res*., *104*, 18,409–18,429, 1999.

D. Rothrock and J. Zhang, Polar Science Center, Applied Physics Laboratory, University of Washington, 1013 NE Fortieth Street, Seattle, WA 98195. (zhang@apl.washington.edu)

(Received April 14, 1999; revised November 23, 1999;
accepted November 29, 1999.)